Phase coherence of parametric-decay modes during high-harmonic fast-wave heating in the National Spherical Torus Experiment

J. A. Carlsson, J. R. Wilson, J. C. Hosea, N. L. Greenough, and R. J. Perkins

---

Articles you may be interested in

The contribution of radio-frequency rectification to field-aligned losses of high-harmonic fast wave power to the divertor in the National Spherical Torus eXperiment
Phys. Plasmas **22**, 042506 (2015); 10.1063/1.4916034

High non-inductive fraction H-mode discharges generated by high-harmonic fast wave heating and current drive in the National Spherical Torus Experiment
Phys. Plasmas **19**, 042501 (2012); 10.1063/1.3699364

Advances in high-harmonic fast wave physics in the National Spherical Torus Experimenta)
Phys. Plasmas **17**, 056114 (2010); 10.1063/1.3371956

Edge ion heating by launched high harmonic fast waves in the National Spherical Torus Experimenta)
Phys. Plasmas **12**, 056108 (2005); 10.1063/1.1871953

Fast ion absorption of the high harmonic fast wave in the National Spherical Torus Experiment
Phys. Plasmas **11**, 2441 (2004); 10.1063/1.1651099
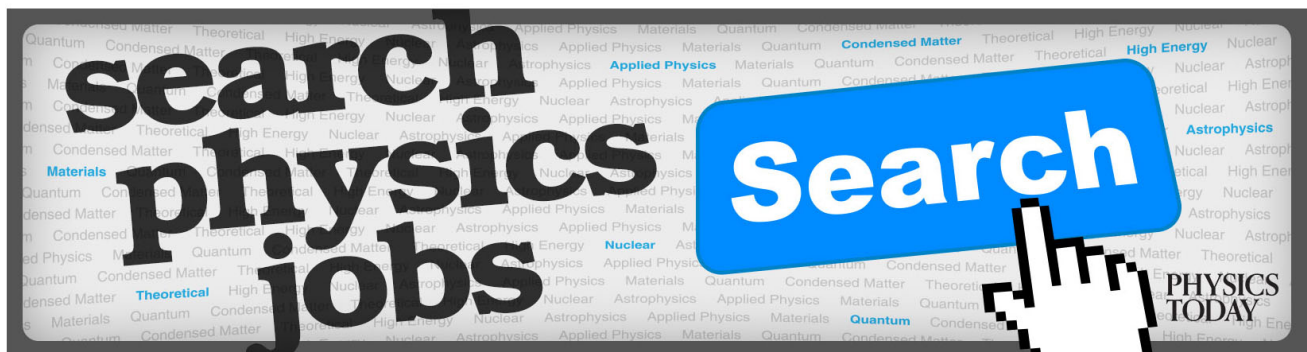
Phase coherence of parametric-decay modes during high-harmonic fast-wave heating in the National Spherical Torus Experiment

J. A. Carlsson,[1,a] J. R. Wilson,[2] J. C. Hosea,[2] N. L. Greenough,[2] and R. J. Perkins[2]
[1]*Crow Radio and Plasma Science, Princeton, New Jersey 08540, USA*
[2]*Princeton Plasma Physics Laboratory, P.O. Box 451, Princeton, New Jersey 08543-0451, USA*

Third-order spectral analysis, in particular, the auto bicoherence, was applied to probe signals from high-harmonic fast-wave heating experiments in the National Spherical Torus Experiment. Strong evidence was found for parametric decay of the 30 MHz radio-frequency (RF) pump wave, with a low-frequency daughter wave at 2.7 MHz, the local majority-ion cyclotron frequency. The primary decay modes have auto bicoherence values around 0.85, very close to the theoretical value of one, which corresponds to total phase coherence with the pump wave. The threshold RF pump power for onset of parametric decay was found to be between 200 kW and 400 kW. *Published by AIP Publishing.* [http://dx.doi.org/10.1063/1.4954825]

I. INTRODUCTION

High-harmonic fast-wave (HHFW) heating is an ion-cyclotron range of frequencies (ICRF) heating scheme developed for high-beta tokamaks[1] and is used at the National Spherical Torus eXperiment (NSTX)[2–4] and the Tokyo Spherical Tokamak-2 (TST-2).[5] The HHFW is susceptible to parametric-decay instability (PDI),[6] where the HHFW pump wave decays into a low-frequency daughter wave and associated sidebands. The low-frequency daughter wave is typically an ion-cyclotron quasi mode (ICQM) and the sidebands either fast waves (FWs) or ion Bernstein waves (IBWs).[6] The intended absorption mechanism for HHFW heating is Landau damping on hot electrons in the plasma core. PDI is undesirable because it can create a parasitic absorption channel, where power is lost in the edge plasma. Also, ICRF heating in conventional tokamaks can be affected by PDI.[7–9]

As for any three-wave resonance, the three PDI modes must conserve energy and momentum

$$f_0 = f_1 + f_2, \ \mathbf{k}_0 = \mathbf{k}_1 + \mathbf{k}_2, \quad (1)$$

respectively, where f is the frequency and $\mathbf{k}$ is the wave vector. The subscript 0 is for the pump wave, and 1 and 2 for the low-frequency and sideband waves, respectively. Second-order spectral analysis, typically the power spectral density, can be used to calculate the amplitude and frequency of plasma modes from probe signals. Frequency matching can then be used to tentatively identify PDI daughter waves. However, frequency matching alone could be accidental, especially in the presence of many modes. If the plasma parameters at the probe location are sufficiently well known, the dispersion relation can be used to calculate the wave vectors from the frequencies to determine whether Eq. (1) is satisfied.

If the wave vectors are not known, phase correlation can instead be used to identify waves related by three-wave resonance,[10] including PDI pump and daughter waves. Unlike

the power spectral density, third-order spectral analysis tools retain phase information and are therefore, in principle, capable of detecting phase correlation.

Two signals $X_a(t)$ and $X_b(t)$, e.g., time traces from probes in a plasma experiment, have correlation

$$C_1(t_1) = \langle X_a(t) X_b(t + t_1) \rangle, \quad (2)$$

where the brackets denote averaging over time t. For two different signals, Eq. (2) is called the cross correlation. For the same signal, $X(t) = X_a(t) = X_b(t)$, it is called the auto correlation. The Fourier transform of the auto correlation is the power spectral density, or power spectrum for short. The power spectrum shows power (amplitude squared) as a function of frequency, but has no phase information. For some applications, such as PDI, the phase contains vital information, making the power spectrum an insufficient analysis tool. For such cases, the second-order power spectrum can be complemented by higher-order spectral-analysis tools. A common choice is the third-order bispectrum, the Fourier transform of the bicorrelation

$$C_2(t_1, t_2) = \langle X_a(t) X_b(t + t_1) X_b(t + t_2) \rangle, \quad (3)$$

where the signals can again be either different (cross bicorrelation) or identical (auto bicorrelation). From the convolution theorem applied to Eq. (3), we get the following expression for the bispectrum

$$B(f_1, f_2) = \hat{X}_a^*(f_1 + f_2) \hat{X}_b(f_1) \hat{X}_b(f_2), \quad (4)$$

where the star superscript denotes complex conjugation.

The value of the bispectrum depends not only on the degree of phase correlation, but also on the amplitude of the Fourier modes. The bicoherence $b(f_1, f_2)$ is a normalized version of the bispectrum that is amplitude independent[10]

$$b^2(f_1, f_2) = \frac{|\langle B(f_1, f_2) \rangle|^2}{\langle |\hat{X}_a(f_1 + f_2)|^2 \rangle \langle |\hat{X}_b(f_1)\hat{X}_b(f_2)|^2 \rangle}, \quad (5)$$

where the normalization is such that $0 \le b^2 \le 1$. $b^2(f_1, f_2) = 0$ when modes with frequencies f_1 and f_2 have completely

a)Present address: Princeton Plasma Physics Laboratory, P.O. Box 451, Princeton, New Jersey 08543-0451, USA Electronic mail: carlsson@pppl.gov

23, 062519-1

uncorrelated phases, and $b^2(f_1, f_2) = 1$ when they are completely phase correlated. As discussed by Lagoutte,[11] the bispectrum is more robust with respect to low signal-to-noise ratio (S/N), but can give false positives, i.e., have large values even without phase correlation. The bicoherence, on the other hand, can give false negatives for phase-correlated signals with low S/N.

The auto bicoherence squared, from Eq. (5) or variants thereof, have been used to identify three-wave resonances in a wide range of plasma types, including low-temperature plasmas,[10] ionospheric/magnetospheric plasma,[11] the H-1 heliac,[12] the HT-7,[13,14] JFT-2M,[15,16] NSTX,[17,18] and TEXTOR[19] tokamaks. For these previous applications, the frequency range was kHz to hundreds of kHz (sub-kHz for space plasmas). In more recent work by Nagashima,[20] bicoherence analysis was applied to HHFW PDI in TST-2. The maximal bicoherence values reported from all these prior studies were in the range of 0.2–0.8. Here, the peak bicoherence values achieved are as large as 0.87, more than a factor of four above the background noise.

In Section II, we present results of second- and third-order spectral analysis of probe data from NSTX HHFW heating experiments, and in Section III, we summarize our findings.

II. RESULTS

The main purpose of the research presented in this paper was to investigate the usefulness of bicoherence for identifying parametric-decay instability in magnetized fusion plasmas, in particular, during HHFW heating in NSTX. A limited set of probe data (from NSTX shots 130595–130608, 130610–130616, and 130618–130622) was analyzed using both second- and third-order spectral-analysis techniques. A comprehensive re-analysis of the full NSTX HHFW-heating data set was beyond the scope of the project, but is currently underway as part of a separate effort and will be reported elsewhere when completed.

The studied shots combine varying levels of HHFW heating, up to 2.5 MW, with 2 MW of neutral-beam injection (NBI). The plasma current was 1 MA for all shots. The on-axis magnetic field was 0.5 T, giving a cyclotron frequency of 3.8 MHz for the majority deuterium ions. At the plasma edge in the outboard midplane, the cyclotron frequency is reduced to 2.7 MHz.

Each of the analyzed shots has data from five different probes: F-G_mid, J-mid, J-top, Reflect, and Edge. The richest data were found to be in F-G_mid, which is also the only probe with high enough S/N to compute the auto bicoherence. J-mid and J-top (and Reflect) each have similar signals, consistent with F-G_mid, but with lower S/N. The signal from the Edge probe is not discernible from noise. The F-G_mid and J-mid probes are located in the outboard midplane. The former between the two central antenna straps and the latter at a toroidal location some distance away from the antenna. Because only one signal from each shot had a sufficiently low S/N, the cross bicoherence between two signals was not computed. The sampling rate was 10^8 samples per second, giving a Nyquist frequency of 50 MHz. An anti-alias filter

had been used with roll-off starting at 40 MHz. The F-G_mid signals have 33×10^6 samples each, J-mid and J-top have 31×10^6, and Reflect and Edge have 30×10^6. The signals were transformed from time to frequency domain using the Fast Fourier Transform (FFT). For the second-order spectral analysis, spectrograms (power spectral density vs. time) were computed, initially using a large window size of 1 ms (10^5 samples) for the FFTs, giving a very high frequency resolution of 1 kHz, but a noisy power spectrum. After an initial data analysis showed that a coarser frequency resolution of 100 kHz would suffice, the FFT window size was decreased to 10^3 samples, and the results from 100 consecutive FFTs were averaged to maintain the 1 ms temporal resolution. This averaging increased the range of detectable signals by almost 10 dB to close to 50 dB, just a few dB below the theoretical limit of about 53 dB set by the quantization error for 16-bit digitization. A -20 dB notch filter at the 30 MHz RF frequency installed before the digitizer could allow even weaker signals to be detected. No other basic signal processing was found to be needed.

For all of the shots analyzed, the NBI was turned on at 75 ms or 150 ms, before the RF, which was turned on after 250 ms.

An example of the power spectrum of a probe signal during RF heating is shown in Fig. 1. It is evident from the spectrogram in Fig. 1(a) that 30 MHz RF heating was turned on at 250 ms and it seems that sidebands (one upper and two lower) and a low-frequency mode appear after about 5 ms, consistent with parametric decay of the RF pump wave. The frequencies match up, with an approximately 2.7 MHz low-frequency mode and upper and lower sidebands at around 30 ± 2.7 MHz. A second, lower sideband at 24.6 MHz can also be seen in the spectrogram. A completely stable, very narrow-bandwidth signal at exactly 5 MHz is present even before the RF was turned on. It is believed to be an artifact of the signal-digitizing process as implemented by the particular analog-to-digital converter that was used.

To minimize the noise of the power spectrum, the signal was averaged over the full RF-heating period (250–330 ms). This average is thus computed using 8000 FFTs on a total of 8×10^6 signal samples. For the given spectral resolution of 0.1 MHz, this procedure should give the maximal S/N. The detectable range for signals was increased accordingly by a few dB to about 51.5 dB, just 2 dB below the theoretical limit for 16-bit digitization. The result is shown in Fig. 2. As can be seen, the noise is significantly reduced compared to the power spectrum shown in Fig. 1(b), which was averaged over a single millisecond. In addition to the modes seen and discussed previously (labeled a, b, f, g, h, and i in Fig. 2), some additional lower-amplitude modes become visible after maximal time averaging, including a second, upper side band at 35.4 MHz (j) and another low-frequency mode at 5.4 MHz (c).

An inherent limitation of the power spectrum is that it only contains information on the frequency and amplitude of the Fourier modes of a signal. The only way to determine if modes are related is to see if their frequencies match up. However, a frequency match alone is not conclusive, since it could be accidental. As will be shown next, third-order
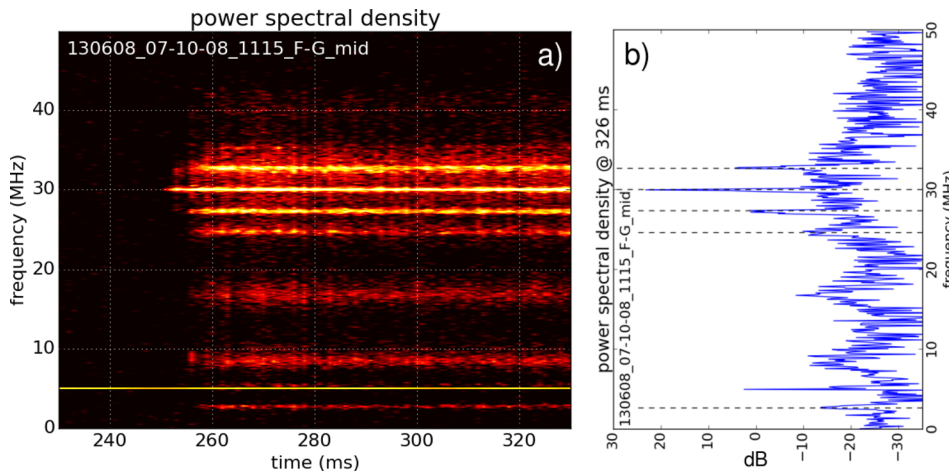
FIG. 1. Spectrogram of shot 130608 F-G_mid probe signal (a), compared to snapshot of power spectrum at 326 ms (b). 2 MW of 30 MHz RF heating is turned on at 250 ms.

spectral analysis (the auto bicoherence, in particular) provides a very useful complement, since it gives the phase correlation between modes, a direct measure of their interrelation.

The auto bicoherence squared, $b^2(f_1, f_2)$ as given by Eq. (5), was computed for the shot 130608 F-G_mid probe signal, again using the maximal time averaging, as described above. The result is shown in Fig. 3. The most notable feature of the contour plot in Fig. 3 is that it has several symmetries and the prominence of the lines $f_1 = \pm 30$ MHz, $f_2 = \pm 30$ MHz, and $f_1 + f_2 = \pm 30$ MHz. To detect parametric decay, phase correlation with the pump wave is of primary importance. To filter out redundant and less interesting information, we therefore look more closely at $b^2(f_1, f_2 = -30$ MHz$)$, along the line indicated by the arrow in Fig. 3. The result is shown as the green graph in Fig. 4. To more easily determine the phase correlation of the modes identified in Fig. 2, the power spectrum, in blue, is plotted over the auto bicoherence squared in Fig. 4. It is confirmed that the suspected primary decay waves a (2.7 MHz), g (27.3 MHz), and i (32.7 MHz) are indeed products of parametric decay of the RF pump wave, with peak values of auto bicoherence squared of $b^2(f_1 = 2.7$ MHz$, f_2 = -30$ MHz$) = 0.74 = 0.86^2$,

$b^2(f_1 = 27.2$ MHz$, f_2 = -30$ MHz$) = 0.75 = 0.87^2$ and $b^2(f_1 = 32.8$ MHz$, f_2 = -30$ MHz$) = 0.68 = 0.83^2$, respectively. The peak locations are sometimes slightly different for power spectrum and bicoherence, respectively, but the variation is within the frequency resolution of 0.1 MHz. The un-squared values of the auto bicoherence for the primary decay modes, in the range 0.85 ± 0.02, are very close to the theoretical value of one for perfect phase correlation with the pump wave. A noisy signal is known to cause a bicoherence that underestimates the true phase correlation and Lagoutte recommends computing the bicoherence averaged over at least several hundred FFTs.[11] The close-to-ideal bicoherence values achieved here is most likely due to averaging over a substantially larger number (8000) of FFTs.

The modes b and c are quite close together, to better separate them, only the low-frequency parts of the auto bicoherence squared and power spectral density are plotted in Fig. 5. As can be seen, mode c is also relatively strongly phase correlated with the RF pump wave (mode h), with the auto bicoherence having a value of 0.74 [$b^2(f_1 = 5.5$ MHz, $f_2 = -30$ MHz$) = 0.55 = 0.74^2$]. As was discussed previously, mode b is probably spurious and definitely not involved in the parametric decay with an auto bicoherence
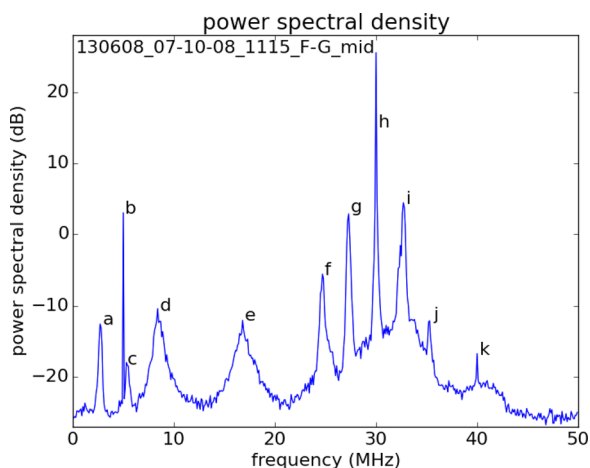

FIG. 2. Power spectral density for the shot 130608 F-G_mid probe signal, averaged over the full, 80 ms RF-heating period. The statistically significant modes are labeled from a to k.
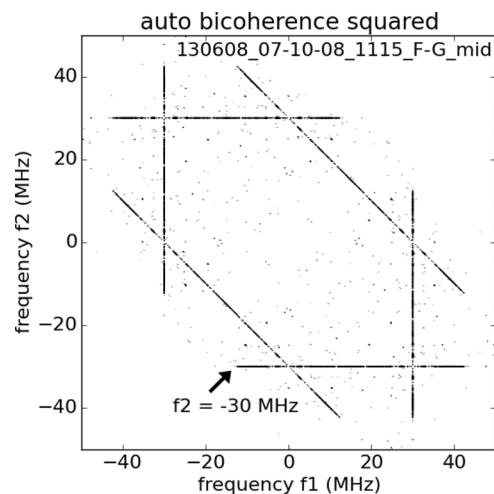

FIG. 3. Auto bicoherence squared for the shot 130608 F-G_mid probe signal, averaged over the full, 80 ms RF-heating period.
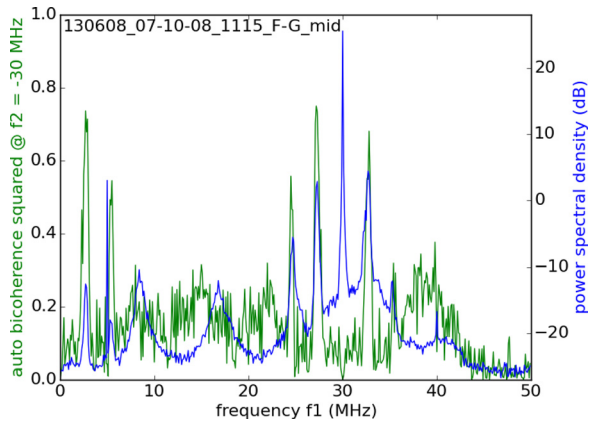
FIG. 4. In green, the auto bicoherence squared for the shot 130608 F-G_mid probe signal along the line indicated by an arrow in Fig. 3. In blue, the corresponding power spectral density from Fig. 2.

FIG. 6. Close up of the sideband-frequency range of Fig. 4. The thin, black, vertical lines shows mode-frequency fits (24.6 MHz, 27.3 MHz, 32.7 MHz, and 35.4 MHz for modes f, g, i, and j, respectively).

value of only 0.21 [$b^2(f_1 = 5.0\,\mathrm{MHz}, f_2 = -30\,\mathrm{MHz}) = 0.04 = 0.21^2$].

Similarly, the bicoherence and power-spectrum graphs are plotted for the sideband-frequency range in Fig. 6. The modes f and j can be identified as secondary lower and upper sidebands. Mode f has an auto bicoherence value of 0.75 [$b^2(f_1 = 24.5\,\mathrm{MHz}, f_2 = -30\,\mathrm{MHz}) = 0.56 = 0.75^2$], virtually identical to that of its sister mode c. Mode j has an auto bicoherence value of 0.56 [$b^2(f_1 = 35.4\,\mathrm{MHz}, f_2 = -30\,\mathrm{MHz}) = 0.32 = 0.56^2$], which is lower than the other daughter waves, but still statistically significant.

In Fig. 4, of the three remaining modes that were labeled in Fig. 2, neither one has a bicoherence value above the noise level. Mode k has a frequency of exactly 40 MHz, which is where the anti-alias filter roll off begins, and might be an artifact of the filtering process. Modes d and e have broad peaks centered at 8.4 MHz and 16.8 MHz, respectively. Their lack of phase correlation with the RF pump wave indicates that they are not involved in the parametric decay, but their exact nature is currently unknown.

Several other shots yield very similar results, e.g., shot 130621, as shown in Fig. 7. The main difference from shot 130608 is that the background signal for shot 130621 is about 10 dB stronger, strong enough to entirely drown out

the spurious mode k. Mode j, the secondary upper sideband, is also only barely discernible.

There is thus ample evidence that parametric decay of the 30 MHz RF pump wave occurs in the studied set of shots with a primary low-frequency mode that is always at 2.7 MHz, an exact match for the local majority-ion cyclotron frequency.

The one possible exception seen in the data set studied here is a brief, 2.5 ms period of shot 130597, as can be seen in Fig. 8. Between 260 and 262.5 ms the RF power is dropped from about 5 dB to −9 dB (see Fig. 8(a)) and the
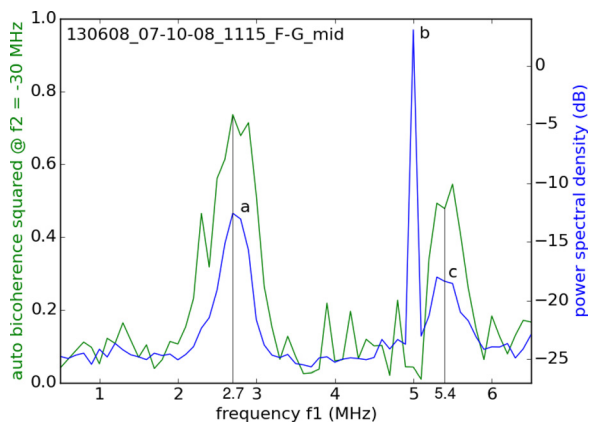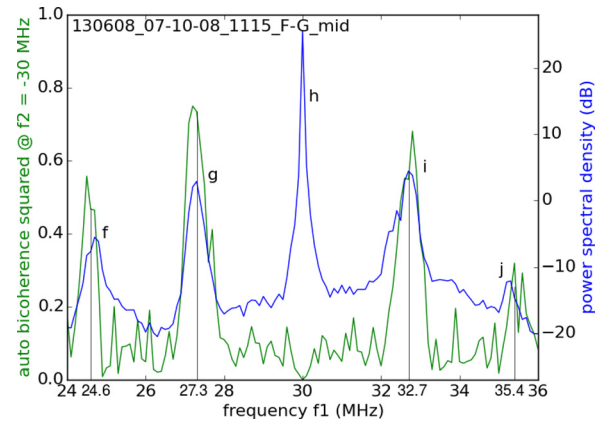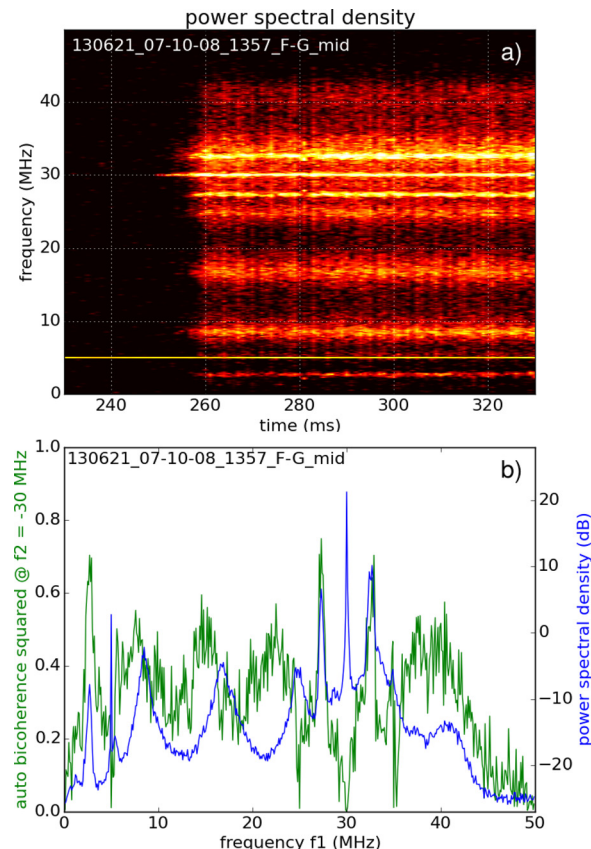

FIG. 5. Close up of low-frequency part of Fig. 4. The thin, black, vertical lines show fits of the mode frequency based on both power spectrum and bicoherence (2.7 MHz for mode a and 5.4 MHz for mode c, respectively).

FIG. 7. Shot 130621 F-G_mid probe signal spectrogram (a) and auto bicoherence squared $b^2(f_1, f_2 = -30\,\mathrm{MHz})$ in green with power spectrum in blue (b).
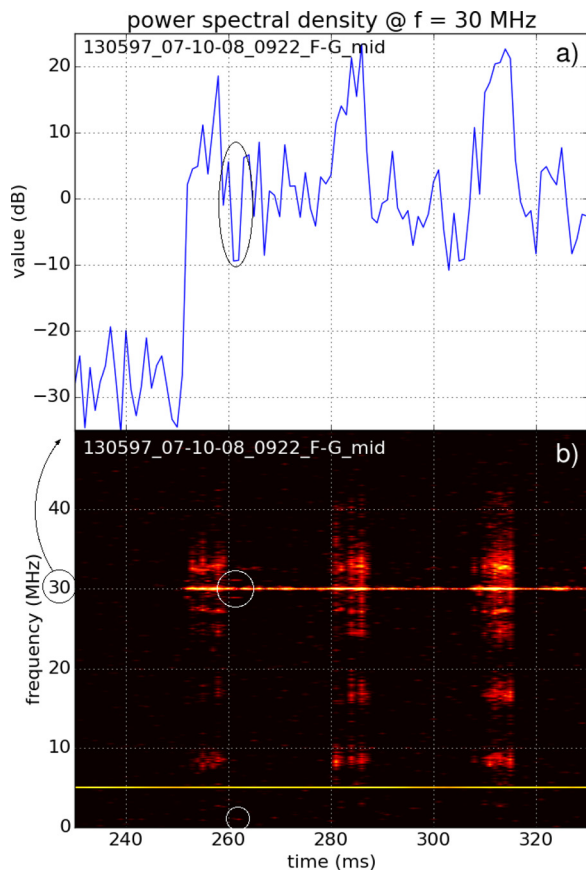
FIG. 8. Shot 130597 power spectral density at 30 MHz vs. time on top (a) and corresponding spectrogram below (b). The circled areas show parametric decay into a lower-frequency daughter wave at 1.1 MHz.

pump wave at 30 MHz splits into three additional modes: 1.1 MHz and 30.0 ± 1.1 MHz, as is shown in Fig. 8(b). However, the S/N of the probe signal is too low for the auto bicoherence to confirm phase correlation and PDI in this case. At TST-2, lower sidebands corresponding to both the 2 MHz majority hydrogen ICQM and an unidentified 600 kHz mode were simultaneously observed.[21] The frequency of the unidentified mode scaled linearly with the magnetic field and it was speculated to be a minority ICQM, possibly for molecular-hydrogen ions.

For all the shots where data were available (except 130622), the RF power is turned on after 250 ms. In some cases, the RF power is held fairly constant for the 80 ms until the probe-signal sampling ends. In other cases, the RF power level is changed several times during the period 250–330 ms. Some examples from this latter category are shown in Fig. 9. The threshold power for onset of PDI could in principle be estimated from these cases from above by finding the smallest RF power level that causes PDI, and from below by finding the largest RF power level that does not cause PDI. For this analysis, we will define the presence of PDI as when the primary low-frequency mode and sidebands are all visible in the spectrograms (in addition to the RF pump wave). With this definition, PDI occurs for shot 130595 only briefly after 300 ms, as can be seen in Fig. 9(b). The power spectral density of the probe signal at 30 MHz (assumed to be proportional to the RF power) during this brief burst of PDI activity reaches almost 20 dB, as seen in Fig. 9(a). Analysing all the similar shots, we arrive at an estimate of the threshold power of 13–16 dB. There seems to be some variability between shots. Compare Figs. 9(c) and 9(d) with Figs. 9(e) and 9(f),
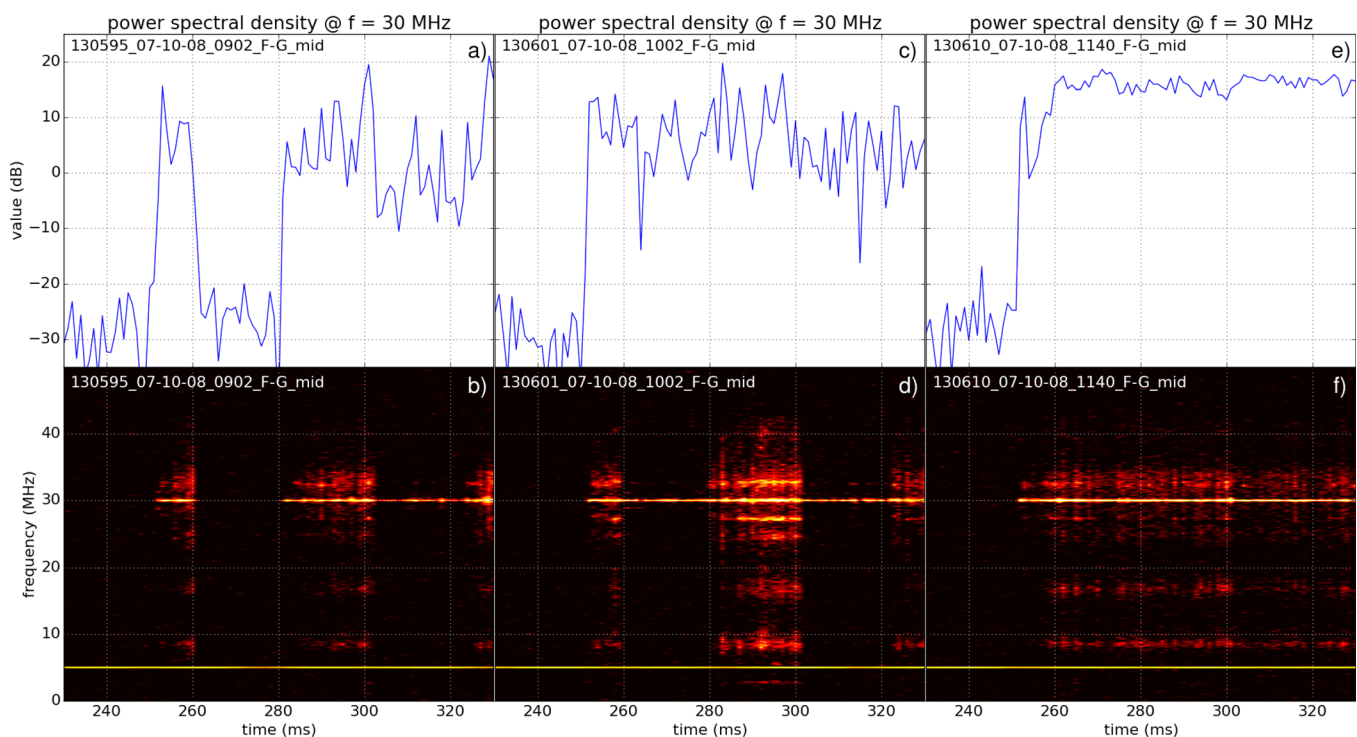

FIG. 9. Shots 130595, 130601, and 130610. Power spectral density at 30 MHz vs. time on top ((a), (c), and (e)) and corresponding spectrograms below ((b), (d), and (f)).

respectively. For the former, clear PDI occurs from 287–301 ms at a power of about 13 dB, whereas for the latter, there is no PDI yet even at a power level of about 16 dB. The maximum power seen in any of the analyzed signal is about 24 dB (not shown), which corresponds to 2.5 MW. Due to the slight variability between shots, the best estimate of the threshold power is thus between 8% (-11 dB) and 16% (-8 dB) of full power, i.e., in the range of 200 kW–400 kW.

III. CONCLUSIONS

Third-order spectral analysis was performed on a set of NSTX probe data from HHFW-heating shots, collected on a single day. Bicoherence values in the range 0.85 ± 0.02 provides strong evidence of phase correlation through parametric decay of the 30 MHz RF pump wave into a low-frequency mode at 2.7 MHz and a 27.3 MHz lower and 32.7 MHz upper sideband. Somewhat lower bicoherence values of 0.74 and 0.75, respectively, for secondary 5.4 MHz low-frequency and 24.6 MHz lower-sideband modes strongly indicate that they also are PDI daughter waves. A 35.4 MHz secondary upper sideband can also be identified, with a bicoherence value of 0.56, about a factor of 2.5 above the noise floor. Second-order spectral analysis, in the form of a spectrogram of the power spectrum, shows that the onset of PDI occurs about 5 ms after the RF is turned on. The threshold RF power for onset of parametric decay was estimated to be between 200 kW and 400 kW (Fig. 9). A spectrogram with 1 ms temporal resolution allowed us to identify a brief (2.5 ms) occurrence of parametric decay into a 1.1 MHz low-frequency mode and 28.9 MHz lower and 31.1 MHz upper sidebands (Fig. 8).

The bicoherence thus proved to be a valuable complement to the power spectral density for this data set, because some necessary requirements were met. To avoid false negatives, i.e., bicoherence values much less than unity despite phase correlation, a large set of samples with high S/N is needed. By tolerating a relatively coarse frequency resolution of 100 kHz, FFTs could be performed on small subsets of 1000 samples at a time. The total sample set from the 80 ms RF heating period then resulted in 8000 FFTs over which to average the bicoherence. This extensive averaging is the primary reason bicoherence values came so close to the ideal value of one for the phase-correlated modes. In contrast, the 2.5 ms episode during shot 130597 of PDI with a 1.1 MHz low-frequency daughter wave, with primary sidebands, only produced 250 FFTs resulting in a bicoherence that was indistinguishable from noise (not shown).

PDI is a particularly suitable target for bicoherence analysis because the pump frequency is known, effectively making the bicoherence a function of a single variable. Plots of the bicoherence at the pump frequency, with the power spectrum overlaid, are a convenient presentation format for PDI data (see Figs. 4–6). The techniques and tools introduced here, and applied to probe data from a representative handful of shots, are currently being used to revisit a larger, more

complete NSTX HHFW-heating data set. The findings from the comprehensive analysis will be presented elsewhere, once completed.

PDI during HHFW heating in NSTX has been identified before based on second-order (power spectrum) spectral analysis alone.[2–4] The earlier results were obtained at lower magnetic field (with edge majority-ion cyclotron frequency of 2 MHz), and in the absence of NBI, in both deuterium and helium plasmas. Up to three lower sidebands (at 28, 26, and 24 MHz, respectively) were shown[2–4] and up to two low-frequency modes (at 2 and 4 MHz, respectively),[4] but no upper sidebands. A more detailed comparison with both theory and these earlier experimental results will be performed and presented in a future publication.

[1]M. Ono, Phys. Plasmas **2**, 4075–4082 (1995).

[2]J. R. Wilson, S. Bernabei, T. Biewer, S. Diem, J. Hosea, B. LeBlanc, C. K. Phillips, P. Ryan, and D. W. Swain, AIP Conf. Proc. **787**, 66–73 (2005).

[3]T. Biewer, R. Bell, S. Diem, C. Phillips, J. Wilson, and P. Ryan, Phys. Plasmas **12**, 056108 (2005).

[4]J. Wilgen, P. Ryan, G. Hanson, D. Swain, S. Bernabei, N. Greenough, S. DePasquale, C. Phillips, J. Hosea, and J. Wilson, Rev. Sci. Instrum. **77**, 10E933 (2006).

[5]T. Oosako, Y. Takase, A. Ejiri, Y. Nagashima, Y. Adachi, H. Kasahara, T. Yamada, O. Watanabe, H. Tojo, S. Kainaga et al., Nucl. Fusion **49**, 065020 (2009).

[6]M. Porkolab, Fusion Eng. Des. **12**, 93–103 (1990).

[7]R. Van Nieuwenhove, G. Van Oost, J. M. Noterdaeme, M. Brambilla, J. Gernhardt, and M. Porkolab, Nucl. Fusion **28**, 1603 (1988).

[8]R. Pinsker, C. Petty, M. Mayberry, M. Porkolab, and W. Heidbrink, Nucl. Fusion **33**, 777 (1993).

[9]J. C. Rost, M. Porkolab, and R. L. Boivin, Phys. Plasmas **9**, 1262–1270 (2002).

[10]Y. C. Kim and E. J. Powers, IEEE Trans. Plasma Sci. **7**, 120–131 (1979).

[11]D. Lagoutte, F. Lefeuvre, and J. Hanasz, J. Geophys. Res. **94**, 435–442, doi:10.1029/JA094iA01p00435 (1989).

[12]M. Shats and W. Solomon, Phys. Rev. Lett. **88**, 045001 (2002).

[13]G. S. Xu, B. N. Wan, and M. Song, Phys. Plasmas **9**, 150–154 (2002).

[14]G. Xu, B. Wan, M. Song, and J. Li, Phys. Rev. Lett. **91**, 125001 (2003).

[15]Y. Nagashima, K. Hoshino, A. Ejiri, K. Shinohara, Y. Takase, K. Tsuzuki, K. Uehara, H. Kawashima, H. Ogawa, T. Ido et al., Phys. Rev. Lett. **95**, 095002 (2005).

[16]Y. Nagashima, K. Itoh, S. I. Itoh, K. Hoshino, A. Fujisawa, A. Ejiri, Y. Takase, M. Yagi, K. Shinohara, K. Uehara, Y. Kusama, and JFT-2M group, Plasma Phys. Controlled Fusion **48**, A377 (2006).

[17]N. Crocker, W. Peebles, S. Kubota, E. Fredrickson, S. Kaye, B. LeBlanc, and J. Menard, Phys. Rev. Lett. **97**, 045002 (2006).

[18]N. Crocker, E. Fredrickson, S. Kubota, W. Peebles, R. Bell, S. Kaye, B. LeBlanc, and J. Menard, Phys. Plasmas **16**, 042513 (2009).

[19]C. de Meijere, S. Coda, A. Krämer-Flecken, S. Soldatov, M. Albergante et al., Plasma Phys. Controlled Fusion **54**, 105024 (2012).

[20]Y. Nagashima, T. Oosako, Y. Takase, A. Ejiri, O. Watanabe, H. Kobayashi, Y. Adachi, H. Tojo, T. Yamaguchi, H. Kurashina et al., Phys. Rev. Lett. **104**, 245002 (2010).

[21]Y. Adachi, A. Ejiri, Y. Takase, O. Watanabe, T. Oosako, H. Tojo, S. Kainaga, T. Masuda, M. Sasaki, J. Sugiyama, and T. Yamaguchi, Rev. Sci. Instrum. **79**, 10F507 (2008).